ARCHIVES OF ACOUSTICS
20, 1, 77–90 (1995)

ENHANCED BANDWIDTH MULTILAYER TRANSDUCERS FOR IMAGING APPLICATIONS

Q. ZHANG AND P.A. LEWIN

Biomedical Engineering and Science Institute and
Department of Electrical and Computer Engineering
Drexel University, Philadelphia, PA 19104, U.S.A

The operating frequency of the presently used PZT or PZT composite ultrasound imaging transducers is determined by the half wavelength resonance or fundamental thickness mode of vibration. This resonance frequency together with the two quarter wavelength matching layers governs the bandwidth of the transducer and hence control the overall resolution capabilities of the imaging system. This paper describes a new generation of multilayer ultrasound imaging transducers which are intentionally designed for off-resonance operation. The design makes use of the exceptionally wideband properties of the thin PVDF polymer film and offers excellent resolution. Moreover, such non-resonant design allows transducer to produce an image at virtually and clinically relevant frequency and can provide resolution tailored to clinician's needs. In addition, the design examined here offers pulse-echo sensitivity comparable to that achievable using PZT piezoceramic transducers. The design principle of the enhanced bandwidth transducer along with the transducer model specially developed to predict key electromechanical parameters of multilayer transducers is presented. These parameters include insertion loss, pulse-echo sensitivity, impulse response and electrical impedance. A few prototypes of this non-resonant tranducer design were built and tested. The experimental results were found to be in good agreement with those obtained from the computer simulations. Fundamental limitations of the design are pointed out and recommendations for future work are outlined.

1. Introduction

The use of ultrasound in clinical diagnosis has been steadily increasing in the past years. The excellent safety record of ultrasound made it a preferred diagnostic tool in the disciplines of cardiology, obstetrics and gynecology. At present, ultrasound is one of the most frequently employed clinical imaging modalities. This achievement in clinical ultrasound diagnosis can be ascribed, to a certain extent, to the constant advancements made in the transducer technology. However, while transducer design has become more and more sophisitcated., the transducer's basic operation principle remained the same. In other words, currently available ultrasound imaging transducers are all designed for operation at fundamental half wavelength resonance

frequency, which eventually sets the limitation on transducer bandwidth and hence the axial resolution of the image.

This paper presents an alternative design of ultrasound imaging transducers which operate below their resonance frequency. While the design discussed here employs a multilayer structure, it differs significantly from the designs reported in the literature [1 – 7]. Briefly, the multilayer design proposed by YAMAMIZU *et al.* [1, 2] contained two to three polymer films with alternate polarization direction and weighted thicknesses. While this approach broadened the bandwidth of a polymer transducer it also increased the two-way insertion loss [1, 2]. Several groups form United Kingdom and United States have considered folded multilayer approach, in which several identical piezoelectric layers were stacked together with alternating vibration polarity [3 – 5]. Although this approach improved the sensitivity of the transducer through a better electrical matching between the transducer and the transmitting/receiving circuits, it also decreased its resonance frequency. This is because in this construction the resonance frequency of the folded transducer is determined by the overall thickness of the stack [3, 5]. Hence, it appears that any increase in the pulse-echo sensitivity can only be achieved at the expense of the bandwidth. Other multilayer approaches involved the combination of PZT and PVDF layers [6] and the use of active matching layers [7], but all of these designs were based on a half wavelength resonant design approach and employed PZT ceramics as piezoelectric materials.

In contrast, the multilayer transducer design examined here uses multiple piezopolymer films which feature acoustic impedance close to that of the human tissue. The film layers are arranged in such a way that their polarization pattern complies with a given Barker code sequence [8]. Since the transducer operates in a non-resonant mode, it allows image to be produced at virtualy and clinically relevant frequencyl. Also, the use of PVDF polymer film provides a basis to achieve an ultrasound image with the highest possible resolution. Finally, the design analyzed here offers pulse-echo sensitivity comparable to that achievable with PZT piezoceramic transducers.

This paper presents a systematic extension of the work described in [9 – 11]. SUNG's work [9] focused primarily on the application of ultrasound pulse compression technique and hase been carried out using PZT ceramics. Also, since his transducer design required the use of a separate transmitter and receiver, the results presented were not immediately applicable in the medical imaging field. PLATTE's research [10, 11] involved development of the pulse-echo Barker code transducer which is further examined in this paper. While the work described in [10, 11] focused mainly on the experimental approach, the work presented here provides a more systematic investigation of the factors governing Barker code transducer performance. Attention is given to a systematic, step-by-step approach including design, construction and testing of the Barker code transducers. In particular, the principle of operation of the multilayer pulse-echo Barker code transducers is thoroughly explained based on the simulations obtained using specially developed transducer model. This model is

particularly suited to simulate a complex, multilayer structure in the context of medical ultrasonic imaging requirements. Key electromechanical parameters including two-way insertion loss, impulse response and electrical impedance are presented and their importance in optimizing the transducer performance is carefully discussed.

In the following, the operation principle of an alternative non-resonant transducer design is outlined together with a brief description of a transducer model developed in this work. The computer simulations of the behaviour of the switchable Barker code transducers were carried out, and the results were compared with those corresponding to the optimized PZT transducers. Based on the simulation results, several prototypes of the Barker code transducers were fabricated and tested. The experimental results are presented and compared with the data obtained from the computer simulations. Advantages and disadvantages of the proposed transducer design are also discussed.

2. Operation principle of the switchable Barker code transducers

As already mentioned, the switchable Barker code transducers presented here make use of multiple piezopolymer layers, and the polarization pattern of the layers is consistent with a given length of a Barker code sequence. Prior to the presentation of the principle of operation of the switchable Barker code transducers, a brief description of Barker code may be useful.

Barker codes are binary codes named after R.H. BARKER, who developed them for synchronization purpose in digital communication systems [8]. The maximum code length was found to be 13 and Table 1 lists the known Barker codes.

Table 1. The known Barker codes

Length of Code	Code Elements	Peak of autocorrelations
1	+	1
3	++−	3
7	+++−−+−	7
11	+++−−−+−−+−	11
13	+++++−−++−+−+	13

One of the important properties of the Barker codes is that the complementary code can be obtained by reversing the sign of every other element in the original code [10]. This feature was extremely useful in developing a pulse-echo Barker code transducer described here. Fig. 1 shows a schematic diagram of a switchable Barker code transducer. The individual piezoelectric layers are stacked according to a Barker code pattern and, for convenience, a Barker code of length 7 is used. The electronic switches connected to each piezoelectric layer are operating in the following way. During the transmitting period, the switches are set to "on" position and the resulting equivalent polarization pattern of the transducer is shown in Fig. 1b. Since each

piezoelectric layer is connected electrically in parallel and acoustically in series, the electrical impedance of the transmitter is inversely proportional to the number of active layers. This is important, because, in general, a single layer PVDF transducer exhibits high electrical impedance due to PVDF film's low dielectric constant. This high impedance prevents an appropriate electrical matching between the transducer and a driving circuit, and hence worsens the PVDF transducer's sensitivity. The use of switches in Fig. 1 improves the electrical matching and hence the transmitting sensitivity of the switchable Barker code transducer. In the receiving mode, the switches are set to "off" position, and the equivalent transducer configuration is shown in Fig. 1c. It is worth noting that since the individual piezopolymer layers are connected electrically in series during the receiving period, the transducer presents a high impedance to the receiver's input. Also, the polarization pattern of the switchable Barker code receiver mirrors that of the transmitter (see Fig. 1b, c). This lays the foundation for designing a practical pulse-echo transducer with exceptionally wide bandwidth and pulse-echo sensitivity comparable with that achievable with the currently available conventional PZT scanheads. The principle of operation of the switchable Barker code transducer can be conveniently explained by referring to Fig. 2.

When the excitation voltage is applied to the transmitter, an acoustic wave is generated in each piezoelectric layer (see Fig. 2; all layers have identical thickness). To simplify the analysis, it is assumed that the interrogated medium is linear and lossless. The generated acoustic pulses are launched into the medium with a delay governed by the propagation time of an acoustic wave through a given number of piezoelectric layers. When the transmitted waves arrive at the surface of the Barker code receiver, they sequentially generate electrical voltage in each individual piezoelectric layer in the receiving assembly. Since the polarization pattern of the receiver mirrors that of the transmitter (see Fig. 1), there will be a time, say $t=tp$, when each of the individual acoustic waves or pulses launched will reach its corresponding receiving layer. When this occurs, the voltage generated in each individual layer will exhibit the same polarity. Consequently, the output voltage produced at the terminals of the Barker code receiver will be n times larger than that generated by a single layer (see Fig. 2). At all other times, the voltage generated in each individual layer exhibits different polarity and some of the voltages are canceled out. The remaining voltages manifest themselves as ripples in the output waveform of the Barker code transducer (see Fig. 2). As a result, the sensitivity of the switchable Barker code transducer is proportional to the number of active layers, and its bandwidth is determined by the thickness of a single layer in the assembly.

In the next section, computer simulations along with a transducer model developed in the course of this work are presented. The results of the computer simulations of the multilayer assembly are compared with those corresponding to the optimized PZT transducer.

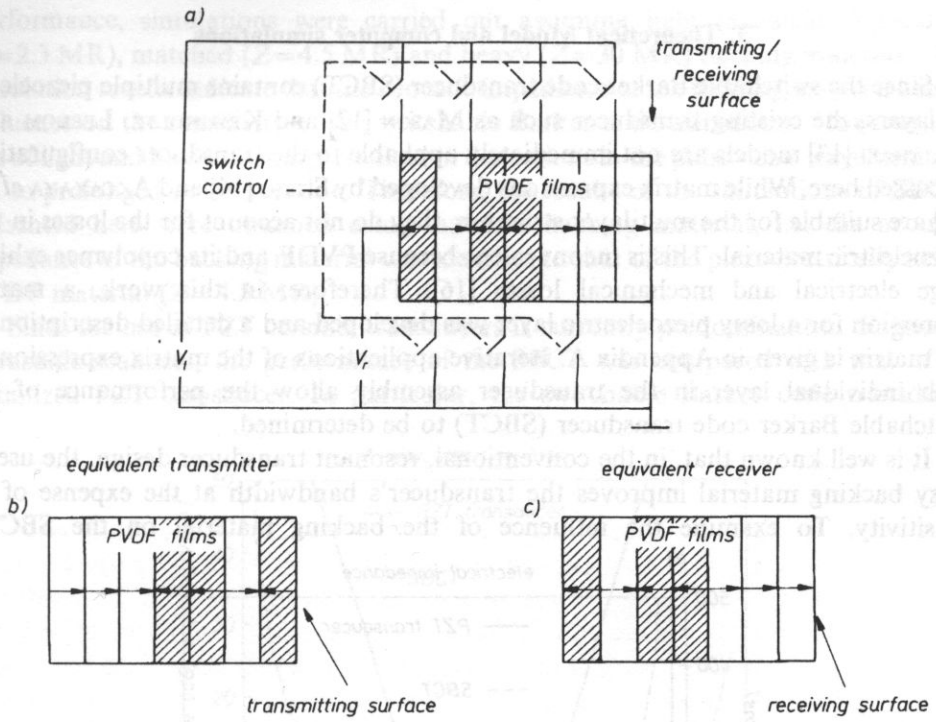

Fig. 1. A schematic diagram of a 7 layer switchable Barker code transducer SBCT. a) Switchable Barker Code Transducer; b) Equivalent polarization pattern of a SBCT transmitter; c) Equivalent polarization pattern of a SBCT receiver; → — polarization direction *Vt* — excitation voltage, *Vr* received voltage.

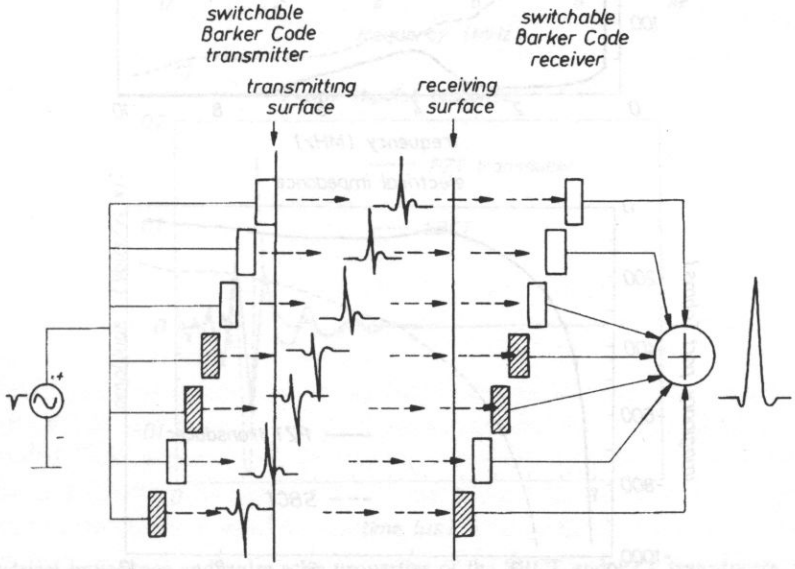

Fig. 2. Principle of operation of Switchable Barker Code Transducers SBCT.

3. Theoretical Model and computer simulations

Since the switchable Barker code transducer (SBCT) contains multiple piezoelectric layers, the existing transducer such as MASON [12] and KRIMHOLTZ, LEEDOM and MATTHAEI [13] models are not immediately appliable to the transducer configuration discussed here. While matrix expressions developed by SITTIG [14] and AKCAKAYA *et al.* [15] are suitable for the multilayer structure, they do not account for the losses in the piezoelectric material. This is inconvenient because PVDF and its copolymer exhibit large electrical and mechanical losses [16]. Therefore, in this work, a matrix expression for a lossy piezoelectric layer was developed and a detailed description of the matrix is given in Appendix A. Iterative applications of the matrix expression to each individual layer in the transducer assembly allow the performance of the switchable Barker code transducer (SBCT) to be determined.

It is well known that, in the conventional, resonant transducer design, the use of lossy backing material improves the transducer's bandwidth at the expense of its sensitivity. To examine the influence of the backing material on the SBCT's

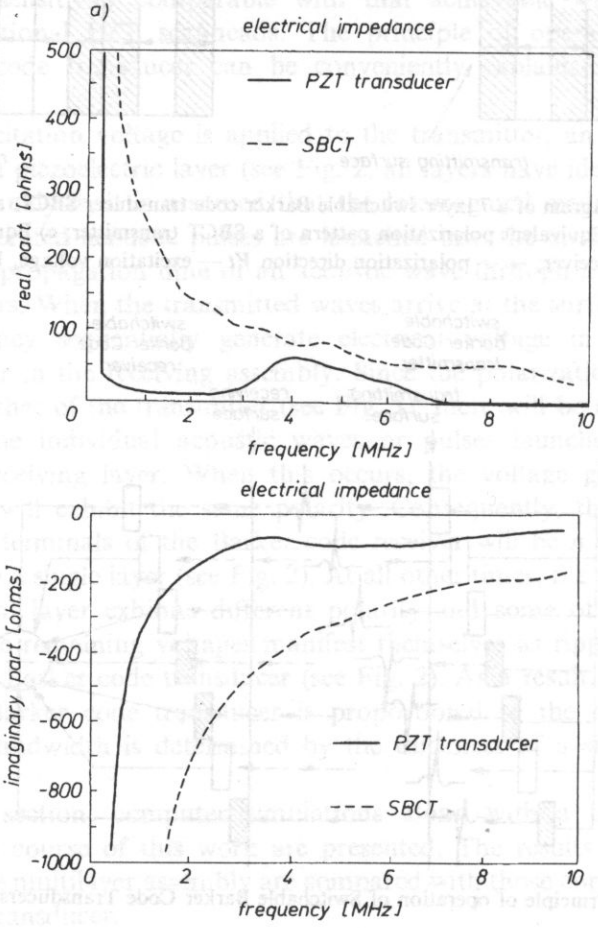

performance, simulations were carried out assuming light (acoustic impedance: $Z=2.3$ MR), matched ($Z=4.5$ MR) and heavy ($Z=30$ MR) backing materials. The simulation results indicate that the acoustic impedance of the backing material has no influence on the sensitivity of the switchable Barker code transducer. However, the use of light and heavy backings resulted in distortions in the pulse-echo waveform and led to prolonged pulse duration. Therefore, the results of the simulations of SBCTs presented here were obtained using matched backing material, i.e. the acoustic impedance of the backing material was identical to that of the piezoelectrically active PVDF material ($Z=4.5$ MR).

Since the use of PZT ceramic transducers is currently predominant in diagnostic ultrasonic scanners, the performance of the SBCT was compared with that of an optimized PZT transducer. In particular, the switchable Barker code transducer

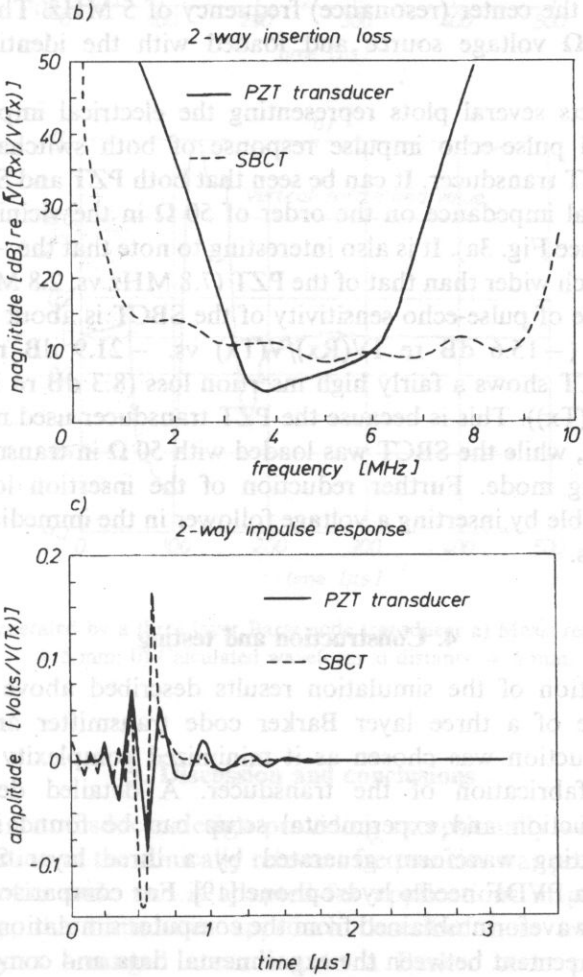

Fig. 3. Electrical impedance and pulse-echo properties of the SBCT and PZT transducers, a) Electrical impedance; b) Two-way insertion loss; c) Pulse-echo impulse response.

simulated here used eleven P(VDF-TrFE) copolymer layers, and was backed by piezoelectrically inactive P(VDF-TrFE) rod. The thickness of a single copolymer layer was 120 μm which corresponds to 10 MHz resonance frequency. It is worth noting that since the switchable Barker code transducer operates in off-resonance mode here, its corresponding center frequency is 5 MHz. In addition, the transducer simulated here was excited by a 50 Ω voltage source and terminated with a 1 MΩ resistance in receiving mode in order to maximize its pulse-echo sensitivity.

The PZT transducer simulated was air backed and used two quarter wavelength front matching layers for optimal performance. The acoustic impedance of these matching layers was chosen based on the procedure suggested in [17]. To facilitate direct comparison between the two designs considered, the PZT transducer operated at the center (resonance) frequency of 5 MHz. The transducer was excited by a 50 Ω voltage source and loaded with the identical resistance in receiving mode.

Figure 3 depicts several plots representing the electrical impedance, two-way insertion loss and pulse-echo impulse response of both switchable Barker code transducer and PZT transducer. It can be seen that both PZT and SBCT transducers exhibit an electrical impedance on the order of 50 Ω in the vicinity of the 5 MHz center frequency (see Fig. 3a). It is also interesting to note that the −6 dB bandwidth of the SBCT is much wider than that of the PZT (7.8 MHz vs. 2.8 MHz). In addition, the peak amplitude of pulse-echo sensitivity of the SBCT is about 6 dB higher than that of the PZT (−15.6 dB re 1V(Rx)/V(Tx) vs. −21.9 dB re 1V(Rx)/V(Tx); However, the SBCT shows a fairly high insertion loss (8.3 dB re 1V(Rx)/V(Tx) vs. 4 dB re 1V(Rx)/V(Tx)). This is because the PZT transducer used matched electrical loads (50 Ω, 50 Ω), while the SBCT was loaded with 50 Ω in transmitting mode and 1 MΩ in receiving mode. Further reduction of the insertion loss in the SBCT transducer is possible by inserting a voltage follower in the immediate vicinity of the piezoelectric layers.

4. Construction and testing

Initial verification of the simulation results described above was carried out using a prototype of a three layer Barker code transmitter and receiver. This three layer construction was chosen as it minimized complexity of the assembly and accelerated fabrication of the transducer. A detailed description of the transducer construction and experimental setup can be found in [18]. Figure 4 shows a transmitting waveform generated by a three layer SBCT transducer and measured by a PVDF needle hydrophone [19]. For comparison, the corresponding transmitting waveform obtained from the computer simulations is also shown in Fig. 4. A good agreement between the experimental data and computer simulations can be seen. The noise observed was traced to be due to an inadequate electrical shielding.

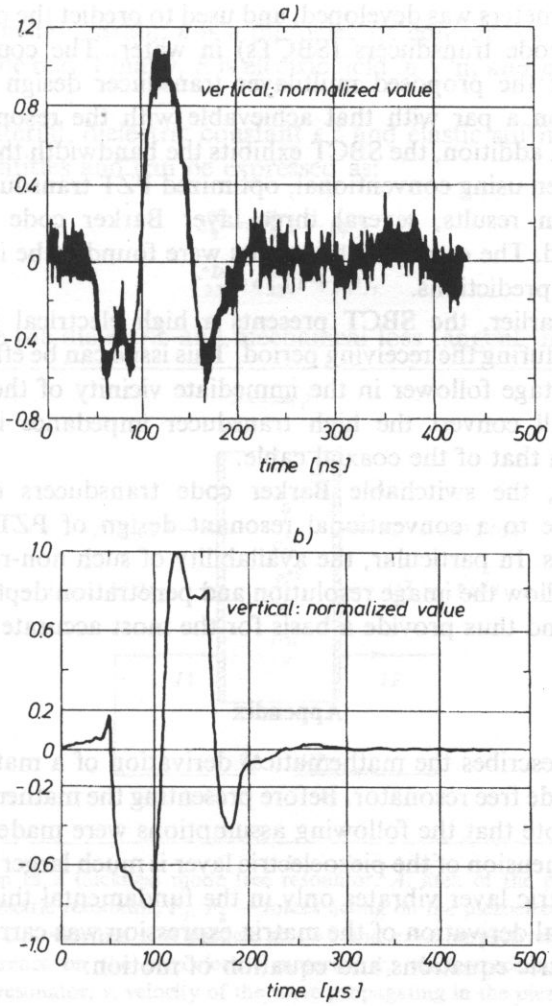

Fig. 4. Waveforms generated by a three layer Barer code transducer a) Measured waveform at distance = 5 mm; b) Calculated waveform at distance = 5 mm.

5. Discussion and conclusions

A non-resonant transducer design providing exceptionally wide bandwidth and suitable for operation at the clinically relevant frequencies was presented. The design makes use of Barker code and is adapted for applications in pulse-echo imaging. More specifically, the transducer approach described here uses multiple active piezopolymer layers arranged according to a Barker code pattern. The work presented here extended the approach published in [10, 11]. In particular, a transducer model capable to predict the transducer behaviour in terms of the relevant

electroacoustic parameters was developed, and used to predict the performance of the switchable Barker code transducers (SBCTs) in water. The computer simulation results indicate that the proposed multilayer transducer design will provide pulse-echo sensitivity on a par with that achievable with the resonant PZT or PZT composite design. In addition, the SBCT exhibits the bandwidth that is twice as large as that obtained when using conventional, optimized PZT transducers. To verify the computer simulation results, several three layer Barker code transducers were fabricated and tested. The experimental results were found to be in good agreement with the theoretical predictions.

As mentioned earlier, the SBCT presents a high electrical impedance to the associated circuitry during the receiving period. This issue can be effectively overcome by integrating a voltage follower in the immediate vicinity of the transducer. This voltage follower will convert the high transducer impedance into 50 Ω output impedance to match that of the coaxial cable.

Once optimized, the switchable Barker code transducers could provide an attractive alternative to a conventional resonant design of PZT ceramic or PZT composite scanheads. In particular, the availability of such non-resonant wideband transducers would allow the image resolution and penetration depth to be tailored to the clinical needs, and thus provide a basis for the most accurate diagnosis.

Appendix

This appendix describes the mathematical derivation of a matrix expression for a lossy thickness mode free resonator. Before presenting the mathematical derivation, it is important to note that the following assumptions were made:

1. The lateral dimension of the piezoelectric layer is much larger than its thickness.
2. The piezoelectric layer vibrates only in the fundamental thickness mode.

The mathematical derivation of the matrix expression was carried out by making use of the piezoelectric equations and equation of motion:

$$T_3 = c_{33}^{*D}\xi_3' - h_{33}D_3, \tag{A.1}$$

$$E_3 = -h_{33}\xi_3' + \frac{D_3}{\varepsilon_3^{*S}}, \tag{A.2}$$

$$-\omega^2\xi_3 = \frac{c_{33}^{*D}}{\rho}\xi_3''. \tag{A.3}$$

The prime indicates differentiation with respect to X_3 which is along the z axis (poling direction) and is normal to the plane of the active piezoelectric layer. T is the stress in N/m^2; c^D is the elastic stiffness constant in N/m^2 measured with D constant; ξ is the particle displacement in direction X_3 in meters; D is the electric flux density in the direction X_3 in C/m^2; ε is the permittivity in F/m (the product of the relative permittivity of the material and the permittivity of a vacuum, 8.85×10^{-12} F/m),

measured under constant strain; h is a piezoelectric constant of the material in N/C and is assumed to be real. Finally, E is electric field in V/m and ρ is the density of the layer in kg/m^3.

For a lossy material, dielectric constant ε^{*S} and elastic stiffness constant c^{*D} are both complex quantities and can be expressed as:

$$\varepsilon_3^{*S}=\varepsilon_3^S(1-j\phi), \tag{A.4}$$

$$c_{33}^{*D}=c_{33}^D(1+j\varphi), \tag{A.5}$$

where ϕ and φ are the dielectric and mechanical loss tangent, respectively.

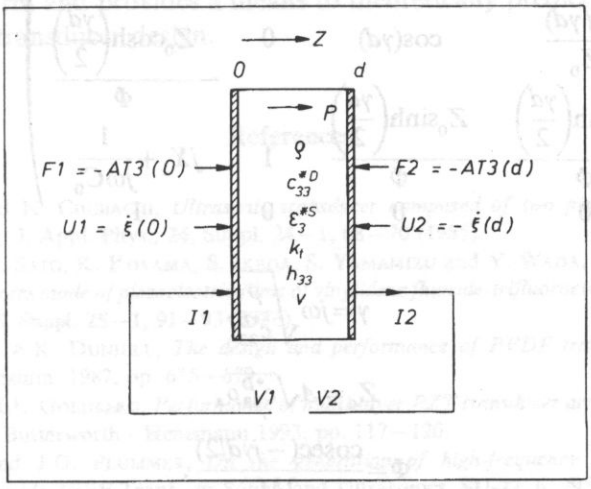

Fig. A.1. Configuration of a thickness mode free resonator. A: area of the piezoelectric material; D: thickness of the piezoelectric resonator; F_1, F_2 — forces acting on the piezoelectric material at $z=0$ and $z=d$, respectively; U_1, U_2: velocities of a particle at $z=0$ and $z=d$, respectively; I_1, I_2: currents due to electric potential difference on the piezoelectric material; k_t: electromechanical coupling factor for thickness mode resonator; v: velocity of the wave propagating in the piezoelectric material.

Fig. A.1 summarizes all forces, displacements, voltages and currents related to a basic thickness mode free resonator.

Using Eq. (A.3) and assuming a harmonic vibration, the amplitude ξ of a particle at z can be expressed as [16]:

$$\xi(z)=\frac{1}{j\omega}\,\frac{U_1\sinh[\gamma(d-z)]-U_2\sinh(\gamma z)}{\sinh(\gamma d)}, \tag{A.6}$$

where U_1 and U_2 are the velocities of the particles at $z=0$ and $z=d$, respectively.

By substituting Eq. (A.6) into Eqs. (A.1) and (A.2) and using the relationships:

$$F_1=-AT_3(0), \tag{A.7}$$

$$F_2=-AT_3(d), \tag{A.8}$$

$$V_1 - V_2 = \int_0^d E_3 dz, \tag{A.9}$$

$$I_1 = I_2. \tag{A.10}$$

the following matrix is obtained:

$$\begin{pmatrix} F_1 \\ U_1 \\ V_1 \\ I_1 \end{pmatrix} = \begin{pmatrix} \cos(\gamma d) & Z_0 \sin(\gamma d) & 0 & -\dfrac{Z_0 \sinh\left(\dfrac{\gamma d}{2}\right)}{\Phi} \\ \dfrac{\sin(\gamma d)}{Z_0} & \cos(\gamma d) & 0 & -\dfrac{Z_0 \cosh\left(\dfrac{\gamma d}{2}\right)}{\Phi} \\ \dfrac{Z_0 \cosh\left(\dfrac{\gamma d}{2}\right)}{\Phi} & \dfrac{Z_0 \sinh\left(\dfrac{\gamma d}{2}\right)}{\Phi} & 1 & jX_1 + \dfrac{1}{j\omega C_0} \\ 0 & 0 & 0 & 1 \end{pmatrix} \begin{pmatrix} F_2 \\ -U_2 \\ V_2 \\ I_2 \end{pmatrix} \tag{A.11}$$

where

$$\gamma = j\omega \sqrt{\frac{\rho}{c_{33}^{*D}}}, \tag{A.12}$$

$$Z_0 = A\sqrt{c_{33}^{*D}\rho}, \tag{A.13}$$

$$\Phi = \frac{\operatorname{cosec}(-j\gamma d/2)}{2M}, \tag{A.14}$$

$$X_1 = Z_0 M^2 \sin(-j\gamma d), \tag{A.15}$$

$$M = \frac{h_{33}}{\omega Z_0}, \tag{A.16}$$

$$C_0 = \frac{A\varepsilon_3^{*T}}{d}. \tag{A.17}$$

Since

$$v = \sqrt{\frac{c_{33}^D}{\rho}}. \tag{A.18}$$

and

$$h_{33}^2 = \frac{k_t^2 c_{33}^D}{\varepsilon_3^S} \text{ [16]}, \tag{A.19}$$

Φ and X_1 can be expressed as:

$$\Phi = \mathrm{j}\,\frac{\omega \mathrm{A}}{2k_t}\sqrt{\rho\varepsilon_3^S(1+j\varphi)}\,\frac{1}{\sinh\left(\dfrac{\gamma d}{2}\right)}, \tag{A.20}$$

$$jX_1 = \frac{k_t^2 v}{\varepsilon_3^S \omega^2 A \sqrt{1+j\varphi}} \sin(\gamma d). \tag{A.21}$$

It should be noted that the matrix of (A.11) can be used to describe layers with both forward and reverse polarization directions as well as piezoelectrically inactive layers by ascribing k_t a positive, negative or zero value, respectively.

Using the electromechanical analogies detailed in [20], it was verified that the matrix given in (A.11) is fully equivalent to the KRIMHOLTZ, LEEDOM and MATTHAEI model [13].

In summary, the matrix expression for a thickness mode free resonator was derived. This expression allows the multiple piezoelectric layers to be described in a mathematical form and provides a means to theoretically predict the performance of the multilayer transducer design.

References

[1] S. YAMAMIZU and N. CHUBACHI, *Ultrasonic transducer composed of two piezoelectric layers with variable weighting*, J. Appl. Phys., **24**, Suppl. 24–1, 68–70 (1985).

[2] K. SAKAGUCHI, T. SATO, K. KOYAMA, S. IKEDA, S. YAMAMIZU and Y. WADA, *Wide-band multilayer ultrasonic transducers made of piezoelectric films of vinylidene fluoride-trifluoroethylene copolymer*, Jap. J. Appl. Phys., **25, Suppl. 25–1**, 91–93 (1986).

[3] M.R. SMITH and A.K. DUNHILL, *The design and performance of PVDF transducers*, Proc. IEEE Ultrasonic Symposium, 1987, pp. 675–679.

[4] S.W. SMITH and R.L. GOLDBERG, *Performance of multi-layer PZT transducer arrays*, proc. Ultrasonics International 93, Butterworth–Henemann 1993, pp. 117–120.

[5] R.G. SWARTZ and J.D. PLUMMER, *On the generation of high-frequency acoustic energy with polyvinylidene fluoride*, IEEE Trans. on Sonics and Ultrasonics, **SU-27**, 6, 295–303 (1980).

[6] L. CHOFFLET and M. FINK, *A multi-piezoelectric structure: The stacked transducer*, Proc. IEEE Ultrasonics Symposium 1991, pp. 611–614.

[7] J.A. HOSSACK and B.A. AULD, *Improving the characteristics of a transducer using multiple piezoelectric layers*, IEEE Trans. UFFC, **40**, 2, 131–139 (1993).

[8] R.H. BARKER, *Group synchronizing of binary digital systems*, in: Communication theory [Ed.] W. Jackson, Butterworth, London 1953, pp. 273–287.

[9] K.M. SUNG, *Piezoelectric multilayer transducers for ultrasonic pulse compression*, Ultrasonics, **22**, 61–68 (1984).

[10] M. PLATTE, *Barker-codierte Mehrschichtwandler aus Polyvinylidenluorid fur den Impuls-Echo-Betrieb mit Ultraschall*, Acustica, **56**, 29–33 (1984).

[11] M. PLATTE, *PVDF ultrasonic transducers*, Ferroelectrics, 75, 327–337 (1987).

[12] W.P. MASON, *Electromechanical transducers and wave filters*, D. Van Nostrand Company, Inc. 2nd Ed. 1948.

[13] R. KRIMHOLTZ, D.A. LEEDOM and G.L. MATTHAEI, *New equivalent circuits for elementary piezoelectric transducers*, Electronics Letters, **6**, 13, 398–399 (1970).

[14] E.K. SITTIG, *Transmission parameters of thickness-driven piezoelectric transducers arranged in multilayer configurations*, IEEE Trans. Sonics and Ultrasonics, **SU-14**, 4, 167–174, (1967).

[15] E. AKCAKAYA, E.L. ADLER and G.W. FARNELL, *Apodization of multilayer bulk-wave transducers*, IEEE Trans. UFFC, **36**, 6, 628–637 (1989).

[16] H. OHIGASHI, *The applications of ferroelectric polymers*, [Eds.] T.T. Wang, J.M. Herbert and A.M. Glass, The Blackie Group Publishers/Chapman and Hill, New York 1988, pp. 236–249.

[17] G.S. De Silets, J.D. Fraser and G.S. Kino, *The design of efficient broad-band piezoelectric transducers*, IEEE Trans. on Sonics and Ultrasonics, **SU-25**, 3, 115–125 (1978).

[18] P.A. Lewin, Q. Zhang and P.E. Bloomfield, *Enhanced bandwidth ultrasound transducers with multiple piezoelectric polymer layers*, in: New developments in ultrasonic transducers and transducer systems, Proc. SPIE 1733, SPIE Washington, USA, 1992, pp. 297–306.

[19] P.A. Lewin, *Miniature piezoelectric polymer ultrasonic hydrophone probes*, Ultrasonics, **19**, 213–216 (1981).

[20] T.F. Hueter and R.H. Bolt, Sonics, Chapt. 4, John Wiley and Sons, 1955.